Journal of Materials Chemistry A

Post-Synthetic Modification of Ionic Liquids Using Ligand-Exchange and Redox Coordination Chemistry

Journal:	*Journal of Materials Chemistry A*
Manuscript ID	TA-ART-06-2020-006195.R2
Article Type:	Paper
Date Submitted by the Author:	12-Oct-2020
Complete List of Authors:	LeRoy, Michael; University of Oregon, Chemistry and Biochemistry and Materials Science Institute Mroz, Austin; University of Oregon, Chemistry and Biochemistry Mancuso, Jenna L; University of Oregon, Department of Chemistry and Biochemistry and Materials Science Institute Miller, Aaron; University of Oregon, Chemistry and Biochemistry and Materials Science Institute Van Cleve, Allison; University of Oregon, Chemistry and Biochemistry and Materials Science Institute Check, Casey; University of Oregon, CAMCOR – Center for Advance Materials Characterization in Oregon Heinz, Hendrik; University of Colorado-Boulder, Chemical and Biological Engineering Hendon, Christopher; University of Oregon, Chemistry and Biochemistry and Materials Science Institute Brozek, Carl; University of Oregon, Chemistry and Biochemistry and Materials Science Institute

SCHOLARONE™
Manuscripts

Post-Synthetic Modification of Ionic Liquids Using Ligand-Exchange and Redox Coordination Chemistry

Michael A. LeRoy[a], Austin M. Mroz[a], Jenna L. Mancuso[a],

Aaron Miller[a], Allison Van Cleve[a], Casey Check[b],

Hendrik Heinz[c], Christopher H. Hendon[a], Carl K. Brozek[a]*

[a]*Department of Chemistry and Biochemistry, Materials Science Institute, University of Oregon, Eugene, OR 97405*

[b]*Center for Advanced Materials Characterization in Oregon University of Oregon, Eugene, OR 97405*

[c]*Department of Chemical and Biological Engineering, University of Colorado—Boulder, Boulder, CO 80309*

Email: cbrozek@uoregon.edu

Abstract: Ionic liquids (ILs) derive their useful properties from molecularly tunable compositions, but methods to diversify anion identities and probe ion speciation remain limited. Here, we demonstrate post-synthetic modification of perhalometallate anions to achieve ionic liquid-to-ionic liquid transformations. Rheological measurements of the metal-containing ILs indicate that minor alterations to anion coordination spheres induces considerable changes to IL viscosities. UV-vis spectra confirm the purities for most ILs, while revealing a surprising cation dependence of perchlorovanadate speciation and supramolecular structure. The intermolecular interactions studied here span a wide range from dispersion to covalent bonding, permitting their impact on IL viscosity to be decoupled and quantified. Together, synthetic strategies from coordination chemistry paired with conventional UV-vis spectroscopy provide a powerful tool for expanding IL compositions and investigating fundamental nanoscale behavior.

Keywords: ionic liquids, supramolecular, intermolecular, coordination chemistry

Introduction

Ionic liquids (ILs) constitute a major class of soft materials, which include IL crystals,[1] polymeric ILs,[2] and porous liquids.[3] As molten salts below 100 ºC, ILs find widespread use as non-aqueous high-concentration electrolyte media with low volatilities, high thermal stabilities, and wide electrochemical windows.[4–7] These "solvent-free" electrolytes can improve the performance of redox flow[8–12] and multivalent-ion batteries,[13] dye-sensitized solar cells,[14–16]

capacitors,[17–19] thermoelectrics,[20–22] and electrocatalysts[23] by enhancing ion mobility[24] or by forming bonds with reactive substrates.[25] In these applications, ILs serve as bulk materials, but their functional properties derive from the molecular composition of the cations and anions. Through competing intermolecular interactions,[26] the constituent ions generate supramolecular structures[27] that govern bulk properties such as viscosity and conductivity.[28] For instance, Kornyshev has proposed that ion composition and molecular steric bulk and ion-pairing produce the non-classical electrical double layer capacitance of ILs.[29–33] Tuning the viscosity and redox behavior of ILs has become increasingly relevant in their use for electrochemical energy storage devices, as these properties govern the transport of charges and ions. Controlling redox potentials and electron transfer kinetics of redox-active ILs is critical to programming device performance, but synthetic strategies remain limited.[9,19] Viscosity must also be tuned with fine precision to be viscous enough to achieve the advantages of solid-state electrolytes, but "soft" enough to ensure rapid transport kinetics.

Despite the importance of molecular composition in controlling the functional properties of ILs, several key challenges remain. First, whereas the vast majority of IL research has explored a wide set of organic cations, novel synthetic routes towards tunable anions would greatly expand available ionic liquid compositions and functional properties. Second, greater insight into the supramolecular structure and molecular speciation of ILs is required for their design as advanced electrolytes, especially at electrode interfaces. Third, we lack general design rules for predicting the magnitude of the effect of specific intermolecular interactions on the bulk behavior of ILs.

Scheme 1A shows common cations and anions incorporated into ILs. The cations are typically organic species, such imidazolium, phosphonium, pyridinium, or sulfonium ions, with

Scheme 1. Representative ions and synthetic routes of ionic liquids.

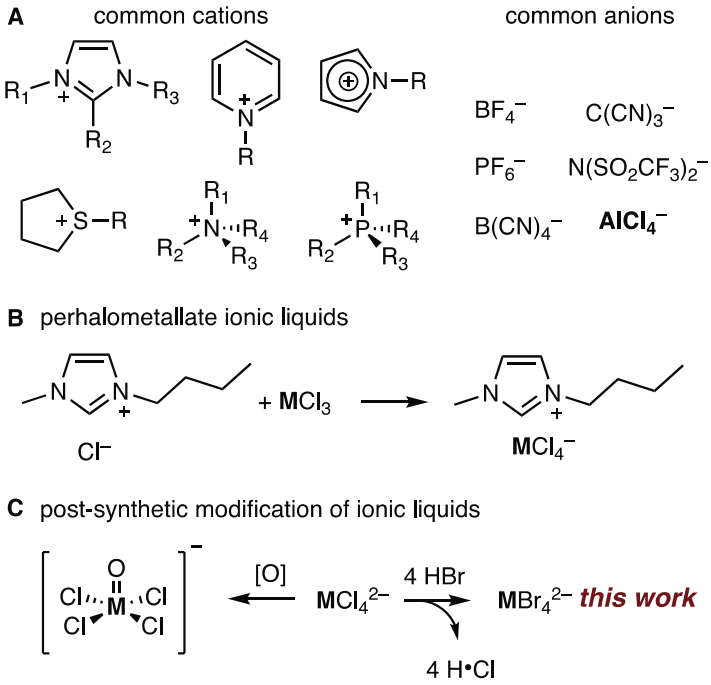

long alkyl chains amenable to functionalization, whereas the anions tend to be inorganic species lacking straightforward tunability. Therefore, while systematic modification of cation functional groups has revealed unexpected relationships between composition and bulk properties, such as the non-linear dependence of viscosity on alkyl chain length,[34] similar studies with anions have not been possible. A promising platform for such structure-property investigations is the perhalometallate anions because they can be prepared with alkaline earth and transition metals, and main group and f-block elements through single-step halide abstraction reactions (Scheme 1B).[13,35–41] To-date, most perhalometallate anion examples include only chloride ligands, however, and little is known about how the composition of these anions dictate supramolecular ordering, which, in turn, controls functional behavior such as viscosity, conductivity, and electrical double layer capacitance. Additionally, certain perhalometallate anions, including $SnCl_3^-$, $ZnCl_4^{2-}$, and $AlCl_4^-$,[13,35,36] exist in dynamic equilibrium with species of varying nuclearities and coordination numbers. Employing these ILs in technologies such as multivalent ion batteries requires

identification of the anion speciation, but current analysis relies on difficult interpretations of Raman spectra. Clearly, alternative synthetic and analytical methods are needed for a molecular understanding of IL function as solvents and electrolytes.

Here, we report post-synthetic modification of perhalometallate anions to achieve ionic liquid-to-ionic liquid transformations and apply electronic absorption spectroscopy for insight into their molecular and supramolecular environments. By treating perhalometallate anions as coordination compounds, we reimagine ligand exchange and redox chemistry as facile tools for precise modification of ILs that can be confirmed through routine UV-visible-NIR measurements. This convenient application of electronic absorption spectroscopy allows insight into the competition between intermolecular interactions, permitting quantification of how variable intermolecular interactions ranging from dispersion to covalent dictate bulk properties such as viscosity. These insights combined with post-synthetic modification provide powerful tools to control IL properties for their application in diverse technologies.

Experimental Section

Materials and Equipment. All manipulations were performed under an atmosphere of nitrogen in an LC Technology Glovebox or by using standard Schlenk techniques. Phosphonium salts, anhydrous VCl_3, and anhydrous VBr_3 were purchased from commercial sources and used without further purification. Hydrated metal salts and imidazolium salts were heated to 100˚C under reduced pressure for 2 days. Tetrabutylammonium hexafluorophosphate ($TBAPF_6$) was recrystallized from ethanol prior to use. Solvents were purified using a LC Technologies SP-1 solvent purification system.

Synthetic Procedures. Synthesis of the materials was carried out by a modification of a literature procedure.[1] In a general procedure the imidazolium or the phosphonium salts were combined with

the corresponding metal halides in a 2:1 molar ratio for divalent metals, and 1:1 molar ratio for trivalent ions, respectively. The mixtures were heated to 100˚C under reduced pressure until a homogeneous mixture was obtained.

Material Characterization. UV-Vis measurements were conducted using a Perkin Elmer Lambda 1050 UV/Vis/NIR spectrometer, with a 150mm InGaAs integrating sphere over 2500-200 nm. Electronic absorption spectra of neat samples were prepared by placing a drop of the ionic liquid between two glass slides. IR spectra were collected on a Bruker Alpha II with an ATR attachment in a nitrogen filled glovebox. X-band EPR spectra were recorded on a Bruker Elexys E 500 at room temperature. Rheological measurements were conducted on a TA Instruments Discovery HR-2 hybrid rheometer, using a Peltier cone plate (Al), 40mm, 1.021˚, and 26-μm truncation gap. Variable temperature rheometry was conducted between 25-200˚C at a shear rate of 10 rad/s. DSC measurements were collected using a DSC 2910 (Du Pont Instruments), cooled with liquid N_2. Electrostatic potential maps were generated by coloring the electron density isosurface plotted up to 0.03 eV/Å^3 according to its electrostatic potential; regions colored red are associated with relatively positive areas of the molecules. IL densities were determined by using the volume displacement method. A graduated cylinder was filled with hexanes as non-polar solvent and weighed. The IL was then added to the graduated cylinder, with the change in volume and mass recorded. Molar volume was calculated by dividing the molecular weight of each IL by their respective densities. X-ray photoelectron spectroscopy measurements were conducted using a ThermoScientific ESCALAB 250 X-ray photoelectron spectrometer.

Results and Analysis

We synthesized a suite of previously reported[38] ILs containing 1-butyl-3-methylimidazolium ([BMIm]$^+$) cations and a variety of perchlorometallate anions based on the

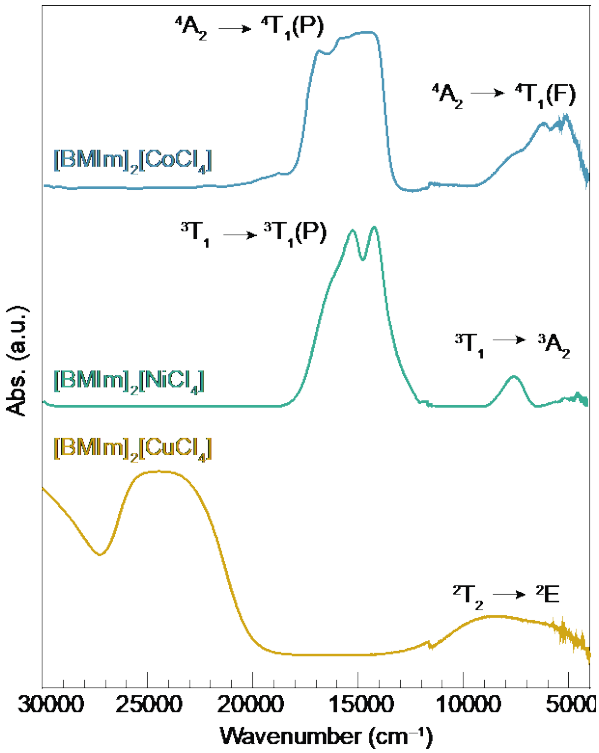

Figure 1: Absorption spectra of neat ionic liquids 1-butyl-3-methylmidazolium (BMIm) perchlorometallate ions. [BMIm]$_2$[CoCl$_4$] in blue, [BMIm]$_2$[NiCl$_4$] in green, and [BMIm]$_2$[CuCl$_4$] in yellow.

hypothesis that, as coordination compounds, these anions would be amenable to redox and ligand-exchange manipulations, although such chemistry had not been demonstrated with ILs. Through facile combination of BMImCl and metal chloride salts in the appropriate stoichiometric ratios, free-flowing colored liquids were generated in single-step routes with proposed formulas BMIm$_x$*M*Cl$_4^{x-}$ (*M* = Cr^{3+}, Fe^{3+}, Mn^{2+}, Co^{2+}, Ni^{2+}, and Cu^{2+}). Determining the purity of ILs typically involves NMR spectroscopy,[42–44] which probes the identity of the organic cations, detects for adventitious water content, and yet applies to only certain perhalometallate anion nuclei, such as ^{119}Sn.[45] Given the propensity of perhalometallates to speciate into complex anionic equilibrium mixtures, we sought analytical methods with broader applicability.

Figure 1 plots electronic absorption spectra of neat ILs composed of [BMIm]$^+$ and CoCl$_4^{2-}$, NiCl$_4^{2-}$, and CuCl$_4^{2-}$ perhallometallate anions. Spectra collected for ILs containing Cr^{3+}, Fe^{3+},

and Mn^{2+} are shown in Figure S1. All spectra in Figure 1 display ligand field (d-d and charge transfer) bands expected of these ions in tetrahedral chloride environments. For precise verification of anion speciation, we performed ligand field analysis to derive the ligand field parameters *Dq*, which measure ligand bonding character, and Racah parameters *B*, which quantifies the interelectronic repulsion experienced by metal d-orbital electrons. As both parameters depend on the geometries and ligand environments of metal ions, they provide exceptional accuracy in assigning metal ion speciation. Analysis of the Co-containing material gives *Dq* and *B* values of 315.82 cm^{-1} and 791.92 cm^{-1} respectively, which agrees with previously reported values for tetrahedral $CoCl_4^{2-}$.[46–48] The spectral bands centered at 15492 cm^{-1} and 5592.5 cm^{-1} can thus be assigned to the $^4A_2 \rightarrow {}^4T_1(P)$ and $^4A_2 \rightarrow {}^4T_1(F)$ transitions, respectively. For the Ni-containing IL, assigning the bands at 14999 cm^{-1} and 7511.7 cm^{-1} to the $^3T_1 \rightarrow {}^3T_1(P)$ and $^3T_1 \rightarrow {}^3A_2$ electronic transitions gives D*q* and *B* values of 408.01 cm^{-1} and 812.76 cm^{-1} respectively. These values are each approximately ~50 cm^{-1} higher than prior analysis of $NiCl_4^{2-}$ ions, but this result can be attributed to distortions in the geometry of the anion.[46,48–50] Finally, assignment of the band at 8337.2 cm^{-1} at for the Cu-containing spectrum to the $^2T_2 \rightarrow {}^2E$ transition of tetrahedral Cu^{2+} gives a *Dq* value of 368 cm^{-1}, which is consistent with a chloride ligand field for a $CuCl_4^{2-}$ with a slight distortion from ideal tetrahedral geometry.[48,51] As expected for metal ions with d^5 electronic configurations, spectra of the Fe^{3+}- and Mn^{2+}-based ILs did not display d-d transitions (Figure S1). Interestingly, the spectrum of the Cr^{3+} IL showed hallmark ligand field bands expected for O_h, rather than T_d, symmetry, suggesting this ionic liquid contains $CrCl_6^{3-}$ instead of $CrCl_4^-$ anions.[52,53] Although water contamination poses a constant threat to IL purity, the sensitivity of these spectra provide clear proof of the absence of water in the metal ion environments. Therefore, electronic absorption spectroscopy serves as a powerful method for understanding IL speciation.

Equipped with a method to probe the coordination environments of IL anions, we sought to demonstrate post-synthetic modification by ligand exchange chemistry. Halide exchange of the $CoCl_4^{2-}$ IL served as an initial target due to the well-resolved spectral bands that would offer convenient handles for monitoring reaction progress. Treating $[BMIm]_2[CoCl_4]$ with aqueous HBr caused an immediate color change from blue to green, consistent with Co^{2+} entering the weaker ligand environment of Br^-. Due to the miscibility of $[BMIm]^+$ with water, however, extraction of the product was difficult, resulting in low yields. Instead, we repeated a similar procedure using trihexyltetradecylphosphonium ($[P_{6,6,6,14}]^+$) as the cation due to its enhanced hydrophobicity. Layering of $[P_{6,6,6,14}]_2[CoCl_4]$ onto a 1-M HBr aqueous solution followed by vigorous shaking resulted in clean separation of a green viscous liquid from the aqueous layer that could be removed by simple decanting. Following drying procedures, successful ligand exchange was confirmed by UV-vis-NIR spectroscopy of the resultant neat ionic liquid, isolated in 65% yield. X-ray photoelectron spectra of this product indicate the presence of Br at energies expected for M-Br bonded species, and the absence of Cl, confirming complete conversion.

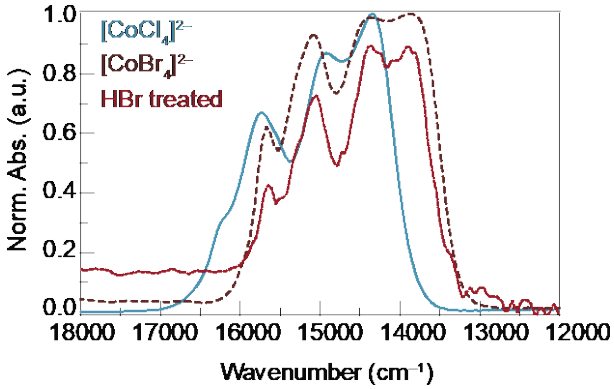

Figure 2: Electronic absorption spectra of neat ionic liquids composed of trihexyltetradecylphosphonium ($P_{6,6,6,14}$) perhalocobaltate ions synthesized directly or through post-synthetic ligand exchange. Spectra in blue and brown correspond to directly synthesized $[CoCl_4]^{2-}$- and $[CoBr_4]^{2-}$-based ionic liquids. The spectrum of the $CoBr_4^{2-}$ prepared through ligand exchange is shown in red.

Figure 2 shows the $^4A_2 \rightarrow {}^4T_1(P)$ transition split by spin-orbit coupling for the product as the red dotted trace, which matches the spectrum of $[P_{6,6,6,14}]_2[CoBr_4]$ prepared directly (brown dashed trace). Both spectra appear red-shifted relative to the spectrum of $[P_{6,6,6,14}]_2[CoCl_4]$ (blue solid trace), which is consistent with the weaker ligand field of Br^-.[54] Interestingly, temperature-dependent viscoelastic measurements of these Co-based ILs evidenced a three-fold decrease in the room-temperature viscosity from 20.77 to 80.96 Pa·s following Br-exchange (Figure S2). The magnitude of this viscosity change is expected between ILs with significantly different cations, but was not expected for anions that only differ in the identity of halides ligands. Additionally,

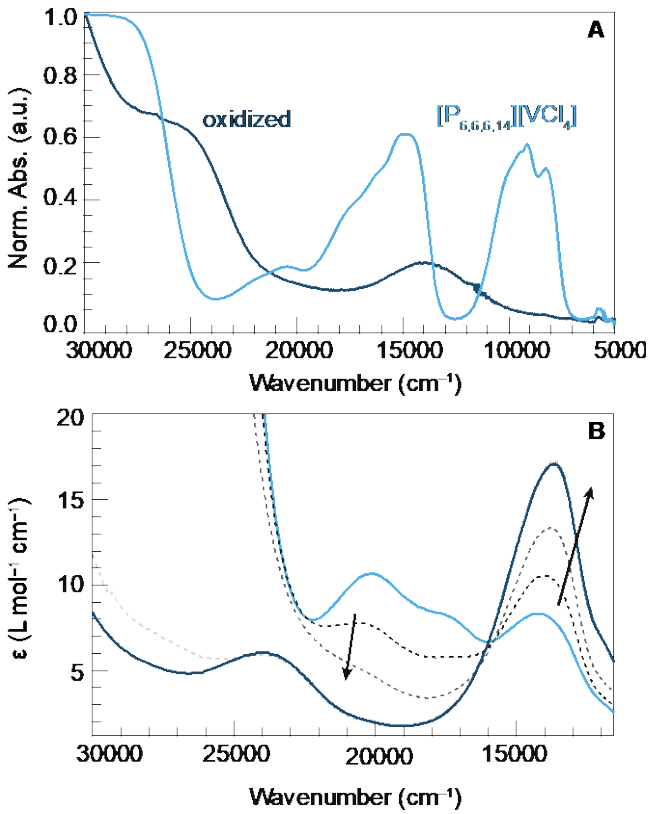

Figure 3: Absorption spectra of $[P_{6,6,6,14}][VCl_4]$ and $[P_{6,6,6,14}]_2[OVCl_4]$ prepared neat (A) and dissolved in MeCN (B). Light blue and green correspond to the $[P_{6,6,6,14}][VCl_4]$ and $[P_{6,6,6,14}][VOCl_4]$, respectively. Data in panel B were collected by preparing a 4.35 mM MeCN solution of $[P_{6,6,6,14}][VCl_4]$ that was kept air-free and then introduced to air. Arrows indicate the direction of spectral evolution.

the viscosities of these ILs are higher than monoanionic chlorometallate ILs,[55–58] which could be attributed to greater Coulombic attraction resulting from the dianionic charges.

To further explore another strategy for post-synthetic modification of ILs, we investigated redox chemistry. In surveying viable perhalometallate anions, vanadium-based ions are noticeably absent the IL literature which we suspected was due to their air sensitivity. To test this hypothesis, we attempted the preparation of [BMIm][VCl_4] in air and observed color changes from violet to dark green, suggestive of aerobic oxidation. Indeed, a UV-vis-NIR spectrum of the resulting neat green liquid displayed absorption bands consistent with V^{4+} in chloride ligand spheres, rather than V^{3+}.[59] Therefore, we reattempted the synthesis of [BMIm][VCl_4] under an inert atmosphere, which resulted in a highly viscous violet material that retained its color indefinitely. For ease of handling, we synthesized an analogous blue IL with $[P_{6,6,6,14}]^+$ cations due to its significantly lower viscosity. Deliberate exposure of this liquid to air caused a single-step color change from blue to green, as evidenced by UV-vis-NIR spectra of the neat material before and after reaction completion (Figure 3A). To verify that the reaction proceeded through a single-step process, a 4.35-mM MeCN solution of [$P_{6,6,6,14}$][VCl_4] was prepared in an air-free cuvette, opened to atmosphere, and

Scheme 2. Proposed redox reaction involving VCl_4^--based ionic liquids in air.

$$4[VCl_4]^- + O_2 + 4H_2O \longrightarrow 4[O{=}VCl_4]^{2-} + 4H^+ + 2H_2O$$

monitored by UV-vis spectroscopy over a 5-hour period whereby the solution turned from light purple to light green (Figure 3B). Indeed, the time-evolved spectra reveal an isosbestic point, indicating a single-step reaction that proceeds only by introduction of air. Interestingly, this reaction requires both moisture and O_2. Based on previous mechanistic studies of VCl_3 oxidation to vanadyl ions, we propose the mechanism shown in Scheme 2.[60,61] Comparison of the data in Figure 3 to spectra of vanadium-chloride eutectic mixtures suggested the oxidation of V^{3+} to V^{4+} to generate a vanadyl-based ionic liquid.[62–65]

Confirmation of vanadium oxidation and generation of a V=O vanadyl moiety was achieved by measuring ATR-IR and X-band EPR spectra of $[P_{6,6,6,14}][VCl_4]$ before and after air exposure. Comparison of the IR spectra shows the growth of a band around 1000 cm^{-1}, which is consistent with literature reports for V=O stretching modes (Figure 4A).[66] Whereas $[P_{6,6,6,14}][VCl_4]$ is EPR silent, as expected for S=1 from a d^2 electronic configuration, the air-exposed product displays the characteristic splitting pattern for V^{4+} resulting from a d^1 configuration with hyperfine splitting to a nuclear spin of I=7/2 (Figure 4B).[63,67] Whereas an octahedrally symmetric V^{4+} center would display an eight-line pattern, the data in Figure 4B show additional peaks that would arise from the axial symmetry of a vanadyl chloride anion. To distinguish between $O{=}VCl_4^{2-}$ and

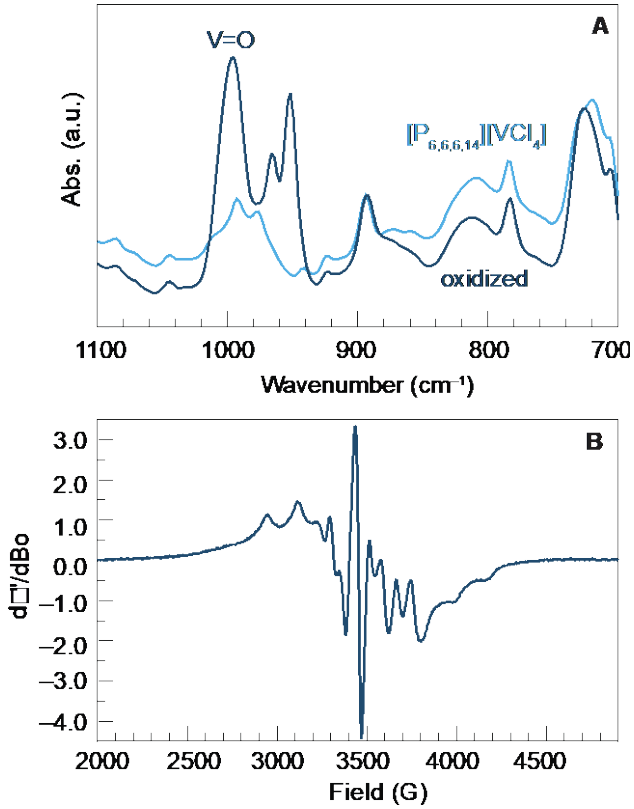

Figure 4: Spectroscopic evidence for post-synthetic conversion of VCl_4^- ions into $OVCl_4^{2-}$. (A) ATR-IR spectra of $[P_{6,6,6,14}][VCl_4]$ (blue) and $[P_{6,6,6,14}]_2[VOCl_4]$ (green). (B) X-band EPR spectrum of $[P_{6,6,6,14}]_2[VOCl_4]$. Neat ionic liquids were used for all measurements and air-free. EPR data were collected at 25°C with a microwave frequency of 9 GHz.

$O{=}VCl_3^-$ as the resulting IL anion, time-dependent density functional theory (TD-DFT)

calculations were performed and compared to the experimental spectrum of the neat material (Figure S13). The additional bands at 22,000 cm^{-1} and 7,000 cm^{-1} predicted for the $O{=}VCl_3^-$ anion suggests $[P_{6,6,6,14}]_2[VOCl_4]$ as the true identity. Redox activity of $[P_{6,6,6,14}][VCl_4]$ was further explored by cyclic voltammetry. Variable scan rate data were collected air-free using MeCN solutions of $[P_{6,6,6,14}][VCl_4]$. Traces in Figure S3 display several electrochemically irreversible reduction and oxidation waves akin to data previously reported for vanadium-chloride electrolytes employed in redox flow batteries.[68,69] We tentatively assign the wave at ~ –0.3 V (vs. Ag wire) to the $V^{3+/2+}$ couple, and the waves at ~ 0.3 V and ~ 0.8 V to the $V^{3+/4+}$ and $V^{4+/5+}$ couples, respectively. Room temperature viscosity measurements of $[P_{6,6,6,14}][VCl_4]$ and $[P_{6,6,6,14}]_2[VOCl_4]$ gave values of 5.07 Pa·s and 2.59 Pa·s respectively.

To explore the generality of redox as a post-synthetic modification technique for ILs, we revisited a prior report on the oxidation of 1-hexyl-3-methylimidazolium ($[HMIm]^+$) $[SnCl_3]^-$ ILs.[57,70] After repeating the reported air-free synthesis, ^{119}Sn NMR of neat $[HMIm][SnCl_3]$ displayed shifts of –128.9 and –138.9 ppm (Figure S4), consistent with Sn^{2+} nuclei and the previously reported values. Deliberate exposure of this ionic liquid to air produced a waxy material confirmed to be $[HMIm]_2[SnCl_6]$ by ^{1}H NMR[71] and ^{119}Sn NMR (Figure S5 and S6).[57,71] Whereas the previous study discussed the structure of the material in its crystalline form, we investigated whether oxidation involved an ionic liquid-to-ionic liquid transformation as well. Indeed, differential scanning calorimetry of neat $[HMIm]_2[SnCl_6]$ displayed a glass transition temperature (T_g) at –54.1 ˚C and a melting point (T_m) at 91.2 ˚C (Figure S7), qualifying this material as a bona fide IL, accessed through post-synthetic redox chemistry. Furthermore, the measured T_g is in good agreement with other chlorostannate ILs.[72]

Macroscopic changes accompanying the systematic modification of these perhalometalle ILs offered a convenient platform for studying the intermolecular interactions that arise from molecular composition and dictate bulk IL properties. In particular, we focused on the strong

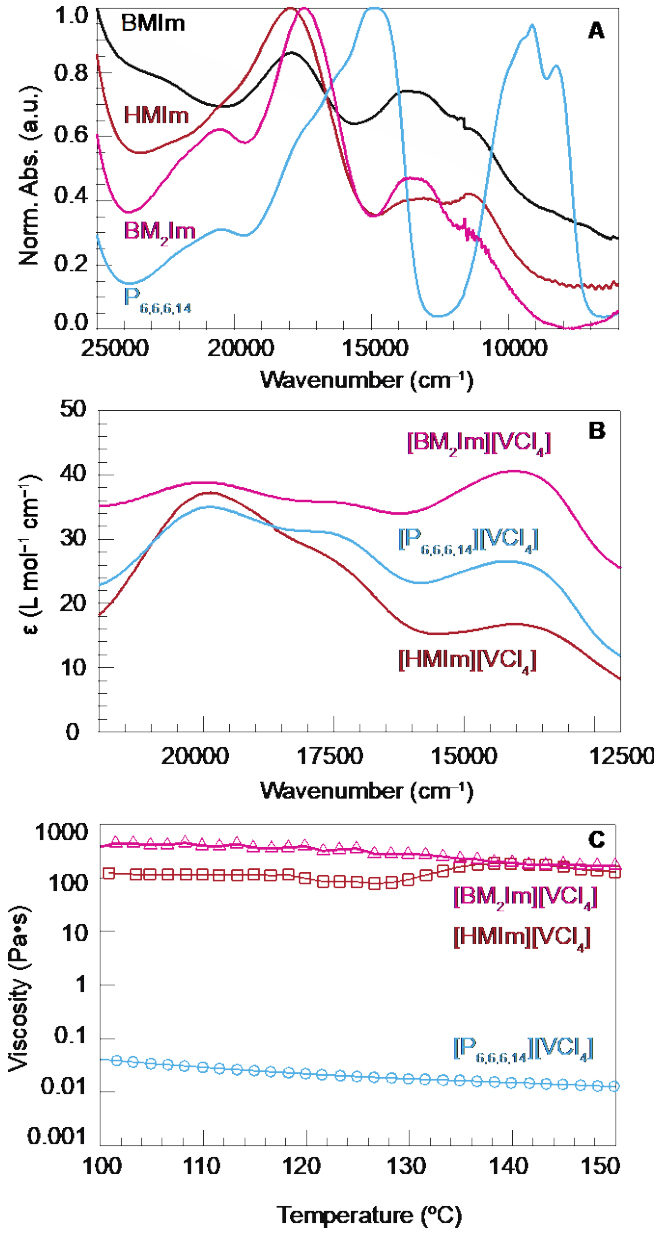

Figure 5: Absorption spectra and temperature-dependent viscosities of ionic liquids based on VCl_4^- with varying cation identities. (A) Absorption spectra of neat ILs. (B) Absorption spectra of IL prepared as 32-mM MeCN solutions (B). **(**C**)** Measurements were collected between 100˚C-150˚C at shear rate of 10 rad/s. 1-hexyl-3-methylimidazolium (HMIm) and 1-butyl-2metyl-3metylimidazolium (BM_2Im) were used for comparison to BMIm- and $P_{6,6,6,14}$-based VCl_4^- ionic liquids.

dependence of coloration and viscosity on the cation identity of the VCl_4^- ILs. Whereas [BMIm][VCl_4] and [HMIm][VCl_4] appeared violet and purple, respectively, [$P_{6,6,6,14}$][VCl_4] was blue. As these colors arise from vanadium-based orbitals, any dependence of the non-coordinating cations was unexpected. UV-vis-NIR spectra of these related materials were collected on neat liquids kept air-free. Indeed, the absorption profiles are considerably different in both peak positions and overall shapes (Figure 5A). Motivated by reports that H-atoms at the 2-position of such imidazolium rings can interact with halides,[73] we hypothesized that weak H–Cl bonding sufficiently perturbed the V^{3+} ligand field to account for such marked spectral differences between the imidazolium and phosphonium derivatives. Therefore, to eliminate the possibility of secondary bonding interactions at the imidazolium 2-position, an analog was synthesized using 1-butyl-2,3-dimethylimidazolium ([BM_2Im]$^+$). By removing such interactions, we expected the resulting spectrum to appear similar to the phosphonium IL. Instead, the spectrum of the resulting indigo [BM_2Im][VCl_4] material appears more similar to the other imidazolium derivatives (Figure 5). To confirm that the cations were responsible for these spectral differences, we dissolved the ILs in acetonitrile, hypothesizing that dilution would eliminate cation-anion interactions through spatial separation. Indeed, UV-vis spectra of the diluted solutions shown in Figure 5B display absorption bands with similar peak energies and shapes, independent of cation identity, confirming that the cations, although intended as non-coordination ions, unexpectedly interact with the $[VCl_4]^-$ anions.

Altering the cation identity of the $[VCl_4]^-$ ILs also induced significant changes in viscosity that accompanied these changes in color. Whereas [$P_{6,6,6,14}$][VCl_4] appears as a free-flowing liquid at room temperature, the imidazolium derivatives exist as waxes until heated near 100 ºC. Figure 5C shows variable temperature viscosities, beginning at 100 ºC. These comparative data show that replacing $[P_{6,6,6,14}]^+$ with imidazolium cations increases viscosity by four orders of magnitude!

Clearly, the intermolecular interactions causing changes in electronic absorption induces strong changes in the supramolecular ordering of the ILs. Although viscosities of the $[BM_2Im]^+$ and $[HMIm]^+$ variants differ considerably, they are more similar than compared to the $[P_{6,6,6,14}]^+$ species, suggesting that the 10,000-fold viscosity difference cannot be due entirely to H–Cl bonding interactions at the imidazolium 2 position. We note that the increase in viscosity of $[HMIm]^+$ above 130˚C can be attributed to the decomposition of the imidazolium cation,[74] which was confirmed by TGA (Figure S24).

To explore whether perchlorometallate ILs exhibit such extreme cation dependencies in general, absorption spectra and variable temperature viscosities were measured for ILs prepared from $[CoCl_4]^{2-}$, $[NiCl_4]^{2-}$, and $[VOCl_4]^{2-}$ and a variety of cations. Figure S8 plots viscoelastic data for $[CoCl_4]^{2-}$, with room temperature values ranging between 6.9–36 Pa·s, a typical range for ILs with different cations. Additionally, the UV-vis-NIR spectra show ligand field bands with similar peak positions and peak shapes. Likewise, the absorption profiles for $[NiCl_4]^{2-}$ ILs with different imidazolium or phosphonium cations appear nearly the same (Figure S9), and various derivatives of $[VOCl_4]^{2-}$ ILs display a similar range of room temperature viscosities (Figure S10). Whereas monoanionic $[VCl_4]^-$ requires only a single charge-balancing cation, however, these cobalt, nickel, and vanadyl materials require two per dianion, which we hypothesized might hinder inter-ion attractive interactions through steric crowding. By this reasoning, $[VCl_4]^-$ might ion-pair effectively with single imidazolium rings and not with bulky phosphonium cations, whereas the dianions might not pair well with any cation due to steric repulsion, leading to a lack of cation dependence. Viscosities of $[FeCl_4]^-$ ILs should, therefore, exhibit a cation dependence akin to $[VCl_4]^-$, but the data in Figure S11 show that viscosities differ by only 0.62 Pa·s between $[HMIm]^+$ and $[P_{6,6,6,14}]^+$ derivatives.

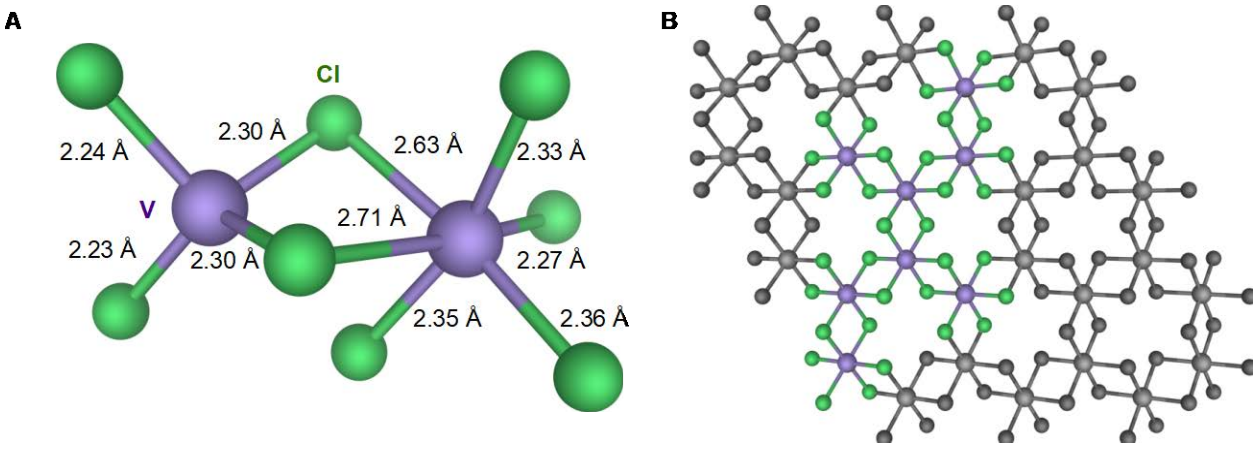

Figure 6: Representations of VCl_x^{y-} oligomers. (A) DFT Geometry-optimized $V_2Cl_8^{2-}$ "dimer". (B) Portion of the VCl_3 crystallographic structure.

Although the cation dependence most likely results from differences in ion pairing, these results, therefore, suggest that the intermolecular interactions arise from chemistry specific to V^{3+}. The structure-induced absorption changes observed for the $[VCl_4]^-$ IL are reminiscent of high-pressure studies involving V^{3+}-doped MgO and Al_2O_3 that showed compression of metal-ligand bonds leading to increased ligand field interactions and concomitant blue shifts to absorption bands.[75] However, whereas uniform compression of all metal-ligand bonds produces simple energetic shifts in the absorption profile of metal ions, the data in Figure 5A show that the presence of imidazolium cations considerably distorts the shapes of the $[VCl_4]^-$ bands. The complex interplay of supramolecular interactions causing the severe cation-dependent optical and viscoelastic properties must therefore cause speciation of V^{3+} into anions that deviate from ideal tetrahedrally symmetric $[VCl_4]^-$ ions.

Given the strong covalency of V^{3+}-Cl^- bonds and the propensity of VCl_3 to form 2D covalent networks,[75] we hypothesize that the synthesis of $[VCl_4]^-$ ILs generates an equilibrium mixture of VCl_x^{y-} aggregates rather than individual $[VCl_4]^-$ monoanions. Figure 6 displays possible representations of the aggregates, including small vanadium dimers (Figure 6A) and larger oligomeric fragments of the 2D VCl_3 lattice with octahedral vanadium ions (Figure 6B). The size

of the oligomers, we propose, depends on the ability of cations to break apart versus stabilize the large anionic clusters. On one hand, the steric bulk and electronegative alkyl groups of $[P_{6,6,6,14}]^+$ might serve to fragment the oligomers, whereas electron-deficient imidazolium rings might better support the formation of VCl_x^{y-} aggregates and give rise to the higher viscosity. The presence of six-coordinate vanadium ions would also explain the blue-shifted absorption bands, as the higher coordination would increase the ligand field strength surrounding V^{3+}.

To investigate the plausibility of VCl_3 aggregation as an explanation for the observed cation dependence, we employed a suite of computational tools. Figure S12 shows computed

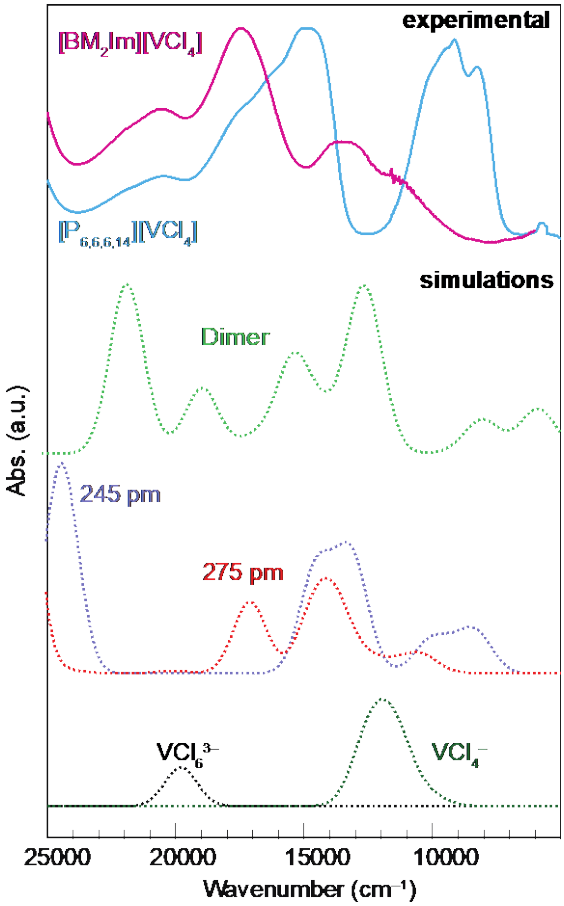

Figure 7: Comparison of experimental and simulated spectra of VCl_x^{y-} ILs. Experimental absorption spectra of $[BM_2Im][VCl_4]$ (pink) and $[P_{6,6,6,14}][VCl_4]$ (blue), Simulated spectra for the $V_2Cl_8^{2-}$ "dimer" (green), simulated spectra of VCl_4^- anions with single V-Cl bonds elongated to 245 (purple) and 275 ppm (red), simulated spectra of idealized VCl_6^{3-} and VCl_4^-.

electrostatic potential (ESP) maps of imidazolium rings with varying alkyl groups and $[P_{6,6,6,14}]^+$. Consistent with previous calculations,[76] and experimental reports on H- and halogen-bonding interactions of anions with imidazolium rings,[77,78] the ESP maps show pockets of electron deficiency at the imidazolium 2 position and ring center, whereas $[P_{6,6,6,14}]^+$ exhibits uniform high electron density. These results support the idea that imidazolium cations could better stabilize VCl_x^{y-} aggregates electrostatically compared to $[P_{6,6,6,14}]^+$. Molecular dynamics simulations performed both with force-fields and *ab initio* methods have elucidated the presence of innumerable configurations of ion pairing in imidazolium-based ionic liquids that span a shallow potential energy surface for their respective chemistries, so we refrained from locating specific geometries of imidazolium-VCl_x^{y-} pairs.[79] Given the complex mixture of possible anion aggregates, Figure 7 plots TD-DFT-simulated absorption spectra in terms of simple limiting case scenarios. First, spectra were computed for VCl_6^{3-} and VCl_4^- with O_h and T_d symmetry, respectively. Clearly, the experimental traces of $[P_{6,6,6,14}][VCl_4]$ and $[BM_2Im][VCl_4]$ cannot be interpreted as a mixture of these two idealized species. Instead, we considered a hypothetical $V_2Cl_8^{2-}$ dimer based on the hypothesis that the equilibrium mixture involves oligomers of six- and four-coordinate vanadium ions. Figure 6A displays the resulting geometry-optimized structure, with each vanadium center distorted considerably from either O_h and T_d symmetry and the idealized bond lengths of 2.461 Å and 2.245 Å, respectively. The corresponding simulated trace is shown in Figure 7. These simulations rule out certain well-defined vanadium species and suggest that the appearance of numerous absorption bands spanning a wide energy spectrum might be explained by the presence of low symmetry V^{3+} oligomers. Inspired by the apparent elongation of V-Cl bonds in the dimer model, we explored whether the experimental spectra could be understood from another simplified scenario of $[VCl_4]^-$ possessing systematically elongated V-Cl bonds

resulting from $[VCl_4]^-$ anion-aggregate interactions. Figure 7 includes simulated spectra for two possible structures where single V-Cl bonds were fixed at 275 pm and 245 pm, while the rest of the geometry was allowed to relax. Interestingly, the shorter V-Cl bond elongation of 245 pm shows better agreement with the $[P_{6,6,6,14}][VCl_4]$ experimental trace, whereas the 275 pm simulation agrees more closely with the $[BM_2Im][VCl_4]$ trace. These results are consistent with the hypothesis that imidazolium cations produce V^{3+} oligomers distorted farther from idealized tetrahedral symmetry.

Discussion

Scheme 3. Summary of ionic liquids examined here with corresponding colors and room temperature viscosities. viscoelastic properties.

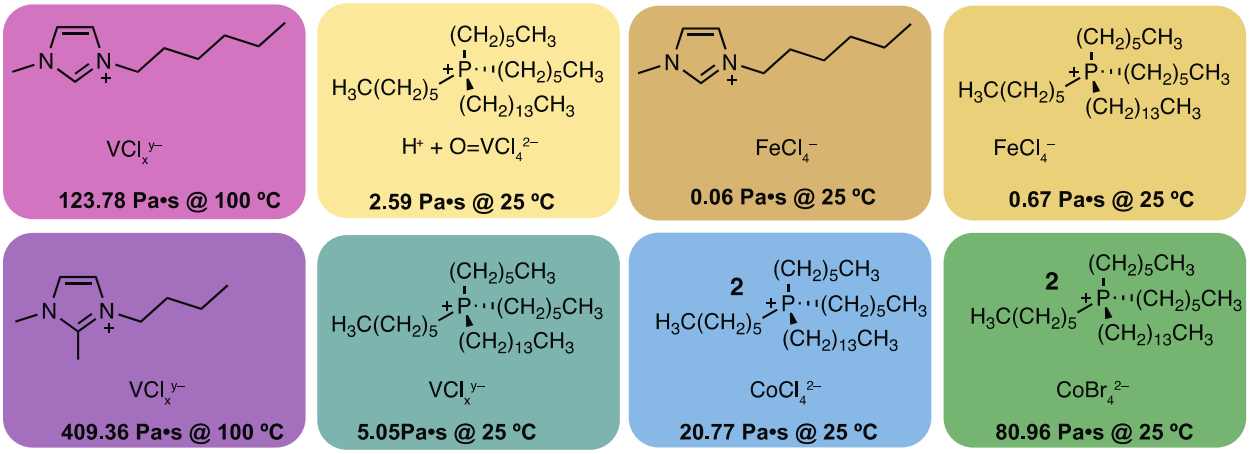

These results indicate that small changes to the coordination chemistry of ILs can yield remarkably different properties in new ILs. Scheme 3 summarizes key differences for some of the ILs reported here that arise in viscosity and color through systematic variation in cation and anion identities. Halide exchange to produce $[P_{6,6,6,14}]_2[CoBr_4]$ from $[P_{6,6,6,14}]_2[CoCl_4]$ caused viscosity to increase by 60.19 Pa·s, which exceeds rheological differences observed through systematic changes to conventional IL ions with more obvious structural differences. For example, the room temperature viscosity of [butylpyridinium][BF_4] differs from [1-propyl-3-

methylimidazolium][BF_4] by only 0.0918 Pa·s, while switching the anion from [butylpyridinium][BF_4] to [butylpyridinium][NTf_2] causes a difference of only 0.1008 Pa·s.[80] Such a large difference from such a minor change to the overall IL composition is surprising. Although anion aggregation could account for higher viscosities and has been observed for $[CoCl_4]^{2-}$ and $[CoBr_4]^{2-}$,[81] the UV-vis spectra suggest the presence of just mononuclear species. Instead, we hypothesize that the greater molecular weight and polarizability of bromide ligands increases viscosity by enhancing halogen bonding and raising the activation energy for viscous flow (E_a). Oxidation of $[P_{6,6,6,14}]_y[VCl_x^{y-}]$ to $[P_{6,6,6,14}]_2[VOCl_4]$ caused a far greater change to viscosity. Whereas elevated temperatures were required to perform rheological measurements on the former, room temperature viscosity of the vanadyl IL produced values of 14.22, 15.27, and 2.59 Pa·s for [BM_2Im], [HMIm], and [$P_{6,6,6,14}$], respectively. These results help quantify the impact of intermolecular interactions on macroscopic properties. In the case of ligand exchange, enhanced secondary bonding interactions altered viscosity 10^2-10^3 times greater than changes between conventional ILs. Disrupting covalent bonding between VCl_x^{y-} oligomers through O-atom transfer, transformed an ionic liquid glass into a free-flowing liquid. Despite the power of this synthetic strategy, it bears few if any literature precedents. One of the few related examples involved anion exchange of halides loosely associated to IL polymers, rather than bound as ligands to metal centers in ILs.[82] The proof-of-concept ligand exchange demonstrated here will inspire future efforts to design ILs based on the exchange of halides for other ligands, such as amides, isothiocyantes, and acetates, as has been well-described for molecular complexes[83–87] and which cannot be accessed as ILs metallate anions through typical routes. Other unconventional ILs based on ligand exchange methods may include mixed-halide anions with variable compositions such as $MCl_{4-x}Br_x^{2-}$, which direct halide-abstraction routes could not access. Practically, the ability of

perhalometallate anions to undergo ligand exchange serves as a cautionary tale for their use in electrochemical energy devices, such as bromine redox flow batteries, where anionic active species may engage in undesirable reactivity with the IL electrolyte.

This work shows that conventional UV-vis spectroscopy enables deep insight into IL nanostructure that otherwise would be difficult to detect. UV-vis spectra have been used in isolated instances to confirm the presence of metal ions extracted into ionic liquids[88] and to understand conversion of metal-containing ionic liquids into coordination polymers,[89,90] whereas this work applies ligand-field analysis to confirm compositional purity and distinguish between mononuclear and polynuclear complexes. Although the solid-like nature of the VCl_4^--based ILs suggested the presence of strong intermolecular interactions, UV-vis allowed specific hypotheses about the nanostructure composition to be tested through comparison to TD-DFT simulated spectra. Perhalometallate aggregation has been detected in ILs based on Sn^{2+}, Al^{3+}, or Zn^{2+},[57,91,92] but could only be detected by subtle differences in Raman spectra. Here, iterative comparison between experimental and simulated spectra pointed to VCl_4^- forming oligomers stabilized by imidazolium ions through secondary bonding interactions.[4,93,94] Recent literature has shown the generation of

Table 1: Viscoelastic and volumetric properties of select ILs prepared here. E_a and PC denote activation energy to viscous flow and packing coefficient, respectively. Room temperature viscosities are reported.

Ionic Liquid	Viscosity (Pa·s)	E_a(kJ/mol)	Free Volume (L/mol)	PC
$[P_{6,6,6,14}]_2[CoCl_4]$	20.77	48.04	0.55	0.72
$[P_{6,6,6,14}]_2[CoBr_4]$	80.96	53.37	0.49	0.76
$[HMIm]_2[CoCl_4]$	6.91	48.67	0.48	0.36
$[BM_2Im]_2[CoCl_4]$	36.53	68.47	0.31	0.46
$[P_{6,6,6,14}][FeCl_4]$	0.670	33.38	0.47	0.52
$[HMIm][FeCl_4]$	0.058	20.68	0.35	0.32

coordination networks derived from ionic liquids,[95] but structural insight required an impressive suite of advanced characterization tools because the polymer contained Zn^{2+} ions silent by UV-vis spectroscopy.[96]

These results explore a range of forces spanning dispersion to covalent bonding, whereas typical reports of ionic liquids focus on manipulating just a few types of intermolecular interactions. Previous reports have shown that rigid supramolecular IL structures, *i.e.* those with stronger, localized interactions exhibit higher viscosities,[97] often showing anisotropic charge distributions within the ion components that cause high viscosities.[98] Such examples of localized and ordered charge pairs allows for enhanced intermolecular interactions through π-π interactions, hydrogen and halogen bonding, and Coulombic forces,[99] but predicting the magnitude of the impact of such interactions remains challenging. Table 1 shows how systematic changes to composition and types of intermolecular interactions impact viscosity and E_a. For example, as discussed above, altering halogen bond interactions in changing from $[P_{6,6,6,14}]_2[CoCl_4]$ to $[P_{6,6,6,14}]_2[CoBr_4]$ causes a minor increase of E_a by ~5 kJ/mol but large jump in viscosity by ~ 40

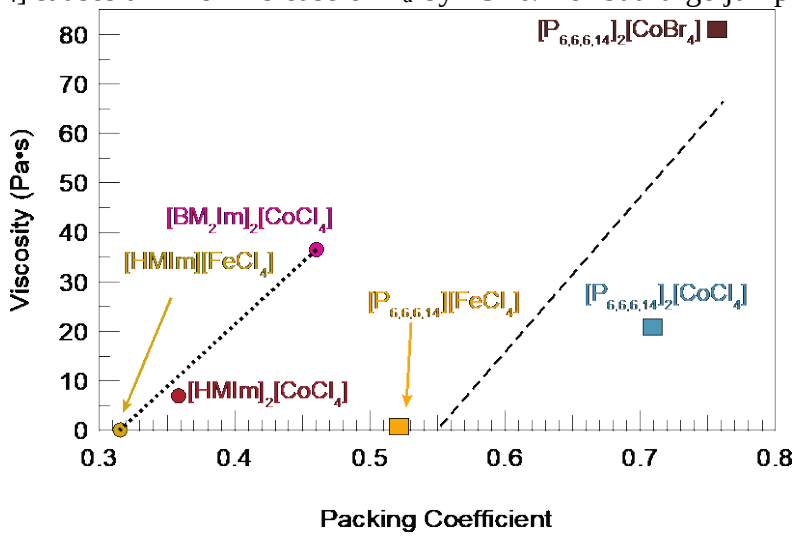

Figure 8: Correlation plot of IL viscosities versus packing coefficient (PC). Room temperature viscosities are reported with constant shear rates of 10 rad/s. Packing coefficients were determined from experimental molar volumes and simulated molecular volumes as detailed in the SI. The dotted and dashed lines denote linear best fits to the imidazolium- and phosphonium-based ILs, respectively.

Pa·s. Altering electrostatic interactions, on the other hand, can be studied by comparing $[P_{6,6,6,14}]_2[CoCl_4]$ and $[P_{6,6,6,14}][FeCl_4]$; by changing from a dianion to a monoanion the electrostatic interactions between and the $[P_{6,6,6,14}]^+$ cation cause E_a to drop by 15 kJ/mol but viscosity drops by more than an order of magnitude. By systematically changing just the cation from a phosphonium to imidazolium, the effect of stronger intermolecular forces such as π-π interactions, hydrogen bonding, and van der Waals interactions becomes readily apparent. The viscosity of $[HMIm]_2[CoCl_4]$ compared to $[BM_2Im]_2[CoCl_4]$ suggest the longer alkyl-chain length and altered dispersion interactions of the former decrease viscosity from ~37 to 7 Pa·s. Comparing $[P_{6,6,6,14}][FeCl_4]$ to $[HMIm][FeCl_4]$ increases viscosity by an order of magnitude, which we attribute to the enhanced halogen-binding interactions of imidazolium ions, corroborated by calculations presented here (Figure S10). It is noteworthy that the low viscosities of these $FeCl_4^-$ materials, in particular the 0.058 Pa·s of $[HMIm][FeCl_4]$, are comparable to ILs used in energy devices, such as the 0.053 Pa·s of BMimTFSI,[19] where performance depends on rapid mass transfer kinetics. In the extreme limit of intermolecular interactions, oxidation of $[P_{6,6,6,14}]_y[VCl_x^{y-}]$ to $[P_{6,6,6,14}]_2[VOCl_4]$ causes viscosity to decrease by 2.48 Pa·s, which we attribute to breaking the covalent VCl_x^{y-} networks. These results, therefore, permit changes intermolecular interactions to be correlated with approximate changes of viscosity, dispersion, halogen bonding, electrostatic, and covalent bonding giving rise to changes on the order of 10^0, 10^1, 10^1, and 10^4 Pa·s, respectively.

Lastly, Table 1 reveals an interesting relationship between IL rheological properties and intermolecular structure. As molecular species that produce bulk behavior, ILs have motivated intense research effort on understanding a physical connection between the intermolecular and macroscopic behavior. These studies have debated whether free volume,[80] molar volume,[100] or molecular volume[28] serve as the most accurate predictor of IL viscosity, ionic conductivity, and

other properties. The data in Table 1 reveals, however, that while these volumetric parameters and E_a exhibit poor correlation with measured room temperature viscosities (Figures S21-S23), higher packing coefficients (PCs) correlate with increased viscosity among ILs with similar cations, i.e., imidazolium versus phosphonium ILs (Figure 8). Typically applied to understanding guest-host supramolecular chemistry, PC is defined as the ratio of molecular volumes to molar volumes, such that dispersion interactions give rise to PC of ~0.55 and H-bonding and stronger interactions increase PC to 0.7 and beyond.[101] Here, we computed the molecular volumes from the electric field, the derivative of the electrostatic potential. This method has demonstrated utility in quantifying the volume and surface area of small polarized molecules,[102,103] while accounting for changes in ionic size due to formal positive and negative charges, as well as highly polarized covalent bonds (see Supporting Information). Whereas volumetric parameters fail to account for intermolecular interactions, PC treats them explicitly. While preliminary, PC appears to be a promising parameter to predict IL macroscopic behavior, such as IL viscosities and conductivities.

Conclusion

We demonstrate that ligand exchange and redox coordination chemistry serve as post-synthetic design strategies for ILs. By tailoring anion composition in a systematic fashion, these methods expand the diversity of ILs, in general, allowing greater control over structure-function relationships. For example, these results indicate that slight changes to perhalometallate coordination spheres result in large changes to bulk rheological properties, suggesting secondary bonding interactions can dominate bulk IL interactions. By employing transition-metal-containing anions, these results also demonstrate that conventional UV-vis spectroscopy enables deep insight into the purity and speciation of the local molecular environment of ionic liquid ensembles. Complex supramolecular assemblies can be modeled by comparing experimental and simulated

spectra. Systematic variation of IL compositions and intermolecular forces permits Coulomb interactions between ions, to be untangled from secondary halogen bonding between terminal chlorides and imidazolium π rings, and dispersion effects. Comparing the effect of these forces reveals the approximate orders of magnitude that each interaction exerts on bulk IL viscosity. Lastly, relating viscosity to packing coefficients shows promise as a novel approach to predicting bulk IL properties. Taken together, these results demonstrate that coordination chemistry provides powerful design and analytical techniques for investigating the fundamental connection of molecular properties to macroscopic behavior.

References

1 K. Goossens, K. Lava, C. W. Bielawski and K. Binnemans, *Chem. Rev.*, 2016, **116**, 4643–4807.

2 H. Nie, N. S. Schauser, N. D. Dolinski, J. Hu, C. J. Hawker, R. A. Segalman and J. Read de Alaniz, *Angew. Chem. Int. Ed.*, 2020, **59**, 5123–5128.

3 A. Knebel, A. Bavykina, S. J. Datta, L. Sundermann, L. Garzon-Tovar, Y. Lebedev, S. Durini, R. Ahmad, S. M. Kozlov, G. Shterk, M. Karunakaran, I. D. Carja, D. Simic, I. Weilert, M. Klüppel, U. Giese, L. Cavallo, M. Rueping, M. Eddaoudi, J. Caro and J. Gascon, *Nat. Mater.*, 2020, *Accepted*, DOI:10.1038/s41563-020-0764-y.

4 S. Zhang, J. Zhang, Y. Zhang and Y. Deng, *Chem. Rev.*, 2017, **117**, 6755–6833.

5 S. Jiang, Y. Hu, Y. Wang and X. Wang, *J. Phys. Chem. Ref. Data*, 2019, **48**, 033101.

6 A. Shakeel, H. Mahmood, U. Farooq, Z. Ullah, S. Yasin, T. Iqbal, C. Chassagne and M. Moniruzzaman, *ACS Sustain. Chem. Eng.*, 2019, **7**, 13586–13626.

7 Z. Lei, B. Chen, Y.-M. Koo and D. R. MacFarlane, *Chem. Rev.*, 2017, **117**, 6633–6635.

8 G. Hernández, M. Işik, D. Mantione, A. Pendashteh, P. Navalpotro, D. Shanmukaraj, R. Marcilla and D. Mecerreyes, *J. Mater. Chem. A*, 2017, **5**, 16231–16240.

9 S. Schaltin, Y. Li, N. R. Brooks, J. Sniekers, I. F. J. Vankelecom, K. Binnemans and J. Fransaer, *Chem. Commun.*, 2016, **52**, 414–7.

10 P. J. Cappillino, H. D. Pratt, N. S. Hudak, N. C. Tomson, T. M. Anderson and M. R. Anstey, *Adv. Energy Mater.*, 2014, **4**, 1300566.

11 A. P. Doherty, *Curr. Opin. Electrochem.*, 2018, **7**, 61–65.

12 L. J. Small, H. D. Pratt, C. L. Staiger and T. M. Anderson, *Adv. Sustain. Syst.*, 2017, **1**, 1700066.

13 M.-C. Lin, M. Gong, B. Lu, Y. Wu, D.-Y. Wang, M. Guan, M. Angell, C. Chen, J. Yang, B.-J. Hwang and H. Dai, *Nature*, 2015, **520**, 324–328.

14 M. Marszalek, Z. Fei, D. R. Zhu, R. Scopelliti, P. J. Dyson, S. M. Zakeeruddin and M. Grätzel, *Inorg. Chem.*, 2011, **50**, 11561–11567.

15 P. Wang, S. M. Zakeeruddin, J.-E. Moser, R. Humphry-Baker and M. Grätzel, *J. Am. Chem. Soc.*, 2004, **126**, 7164–7165.

16 G. P. S. Lau, J.-D. Décoppet, T. Moehl, S. M. Zakeeruddin, M. Grätzel and P. J. Dyson, *Sci. Rep.*, 2015, **5**, 18158–18166.
17 S. Bi, H. Banda, M. Chen, L. Niu, M. Chen, T. Wu, J. Wang, R. Wang, J. Feng, T. Chen, M. Dincă, A. A. Kornyshev and G. Feng, *Nat. Mater.*, 2020, **19**, 552–558.
18 M. Matsumoto, S. Shimizu, R. Sotoike, M. Watanabe, Y. Iwasa, Y. Itoh and T. Aida, *J. Am. Chem. Soc.*, 2017, **139**, 16072–16075.
19 E. Mourad, L. Coustan, P. Lannelongue, D. Zigah, A. Mehdi, A. Vioux, S. A. Freunberger, F. Favier and O. Fontaine, *Nat. Mater.*, 2016, **16**, 446–453.
20 T. J. Abraham, D. R. MacFarlane and J. M. Pringle, *Energy Environ. Sci.*, 2013, **6**, 2639.
21 A. Mazaheripour, S. Majumdar, D. Hanemann-Rawlings, E. M. Thomas, C. McGuiness, L. D'Alencon, M. L. Chabinyc and R. A. Segalman, *Chem. Mater.*, 2018, **30**, 4816–4822.
22 T. J. Abraham, D. R. MacFarlane and J. M. Pringle, *Chem. Commun.*, 2011, **47**, 6260.
23 B. a Rosen, A. Salehi-Khojin, M. R. Thorson, W. Zhu, D. T. Whipple, P. J. a Kenis and R. I. Masel, *Science*, 2011, **334**, 643–644.
24 T. Yamamoto, K. Matsumoto, R. Hagiwara and T. Nohira, *ACS Appl. Energy Mater.*, 2019, **2**, 6153–6157.
25 B. A. Rosen, A. Salehi-Khojin, M. R. Thorson, W. Zhu, D. T. Whipple, P. J. A. Kenis and R. I. Masel, *Science*, 2011, **334**, 643–644.
26 R. P. Matthews, T. Welton and P. A. Hunt, *Phys. Chem. Chem. Phys.*, 2014, **16**, 3238–3253.
27 R. Hayes, G. G. Warr and R. Atkin, *Chem. Rev.*, 2015, **115**, 6357–6426.
28 J. M. Slattery, C. Daguenet, P. J. Dyson, T. J. S. Schubert and I. Krossing, *Angew. Chemie*, 2007, **119**, 5480–5484.
29 M. V. Fedorov, N. Georgi and A. A. Kornyshev, *Electrochem. Commun.*, 2010, **12**, 296–299.
30 Z. A. H. Goodwin and A. A. Kornyshev, *Electrochem. commun.*, 2017, **82**, 129–133.
31 M. V. Fedorov and A. A. Kornyshev, *Chem. Rev.*, 2014, **114**, 2978–3036.
32 A. A. Kornyshev, *J. Phys. Chem. B*, 2007, **111**, 5545–5557.
33 X. Mao, P. Brown, C. Červinka, G. Hazell, H. Li, Y. Ren, D. Chen, R. Atkin, J. Eastoe, I. Grillo, A. A. H. Padua, M. F. Costa Gomes and T. A. Hatton, *Nat. Mater.*, 2019, **18**, 1350–1357.
34 M. A. A. Rocha, C. M. S. S. Neves, M. G. Freire, O. Russina, A. Triolo, J. A. P. Coutinho and L. M. N. B. F. Santos, *J. Phys. Chem. B*, 2013, **117**, 10889–10897.
35 J. Estager, P. Nockemann, K. R. Seddon, M. Swadźba-Kwaśny and S. Tyrrell, *Inorg. Chem.*, 2011, **50**, 5258–5271.
36 M. Currie, J. Estager, P. Licence, S. Men, P. Nockemann, K. R. Seddon, M. Swadźba-Kwaśny and C. Terrade, *Inorg. Chem.*, 2013, **52**, 1710–1721.
37 M. Gjikaj, T. Xie and W. Brockner, *J. Inorg. Gen. Chem.*, 2009, **635**, 1036–1040.
38 Q. Wang, Y. Geng, X. Lu and S. Zhang, *ACS Sustain. Chem. Eng.*, 2015, **3**, 340–348.
39 C. Jagadeeswara Rao, K. A. Venkatesan, K. Nagarajan, T. G. Srinivasan and P. R. Vasudeva Rao, *J. Nucl. Mater.*, 2010, **399**, 81–86.
40 J. Estager, J. D. Holbrey and M. Swadźba-Kwaśny, *Chem. Soc. Rev.*, 2014, **43**, 847–886.
41 R. Kore, P. Berton, S. P. Kelley, P. Aduri, S. S. Katti and R. D. Rogers, *ACS Catal.*, 2017, 7014–7028.
42 H. Weingärtner, *Curr. Opin. Colloid Interface Sci.*, 2013, **18**, 183–189.
43 R. Nanda and K. Damodaran, *Magn. Reson. Chem.*, 2018, **56**, 62–72.

44 A. Noda, K. Hayamizu and M. Watanabe, *J. Phys. Chem. B*, 2001, **105**, 4603–4610.
45 M. Currie, J. Estager, P. Licence, S. Men, P. Nockemann, K. R. Seddon, M. Swadźba-Kwaśny and C. Terrade, *Inorg. Chem.*, 2013, **52**, 1710–1721.
46 N. K. Hamer, *Mol. Phys.*, 1963, **6**, 257–264.
47 J. Ferguson, *J. Chem. Phys.*, 1963, **39**, 116–128.
48 H. A. Weakliem, *J. Chem. Phys.*, 1962, **36**, 2117–2140.
49 G. P. Smith, C. H. Liu and T. R. Griffiths, *J. Am. Chem. Soc.*, 1964, **86**, 4796–4802.
50 D. M. L. L. Goodgame, M. Goodgame and F. A. Cotton, *J. Am. Chem. Soc.*, 1961, **83**, 4161–4167.
51 C. C. Torardi, J. C. Calabrese, R. J. Deeth, M. A. Hitchman, G. Lehmann and H. Sachs, *EPR and Optical Spectra of $CuCl_4$ Doped into Single Crystals of Several Zinc(II) Host Lattices*, 1984, vol. 23.
52 O. S. Wenger, R. Valiente and H. U. Güdel, *J. Chem. Phys.*, 2001, **115**, 3819–3826.
53 J. M. García-Lastra, M. Moreno and M. T. Barriuso, *J. Chem. Phys.*, 2008, **128**, 144708.
54 F. A. Cotton, D. M. L. Goodgame and M. Goodgame, *J. Am. Chem. Soc.*, 1961, **83**, 4690–4699.
55 S. A. Pierson, O. Nacham, K. D. Clark, H. Nan, Y. Mudryk and J. L. Anderson, *New J. Chem.*, 2017, **41**, 5498–5505.
56 C. Chiappe and S. Rajamani, *European J. Org. Chem.*, 2011, 5517–5539.
57 M. Currie, J. Estager, P. Licence, S. Men, P. Nockemann, K. R. Seddon, M. Swadźba, S.-K. Kwaśny and C. C. Terrade, *Inorg. Chem*, 2013, **52**, 1710-1721 .
58 L. C. Brown, J. M. Hogg, M. Swadz´ba and S.-K. Kwas´ny, *Top. Curr. Chem.*, 2017, **375**, 1–40.
59 P. B. Hitchcock, R. J. Lewis and T. Welton, *Polyhedron*, 1993, **12**, 2039–2044.
60 A. Bakač, A. T. Thornton and A. G. Sykes, *Inorg. Chem.*, 1976, **15**, 274–278.
61 P. Buglyó, D. C. Crans, E. M. Nagy, R. L. Lindo, L. Yang, J. J. Smee, W. Jin, L. H. Chi, M. E. Godzala and G. R. Willsky, *Inorg. Chem.*, 2005, **44**, 5416–5427.
62 D. M. Gruen and R. L. McBeth, *J. Phys. Chem.*, 1962, **66**, 57–65.
63 K. R. Seddon, *Electron paramagnetic resonance spectroscopy of vanadium(IV) complexes and related species*, 1980.
64 B. C. Sydney Furman and C. S. Garner, *Absorption Spectra of Vanadium (III) and Vanadium (IV) Ions in Complexing and Non-complexing Media*, UTC, 1934, vol. 3.
65 I. B. Polovov, V. A. Volkovich, S. A. Shipulin, S. V. Maslov, A. A. Khokhryakov, B. D. Vasin, T. R. Griffiths and R. C. Thied, *J. Mol. Liq.*, 2003, **103**–**104**, 387–394.
66 R. C. Bell, A. W. Castleman and D. L. Thorn, *Inorg. Chem.*, 1999, 5709–5715.
67 T. S. Smith, R. LoBrutto and V. L. Pecoraro, *Coord. Chem. Rev.*, 2002, **228**, 1–18.
68 Q. Xu, L. Y. Qin, Y. N. Ji, P. K. Leung, H. N. Su, F. Qiao, W. W. Yang, A. A. Shah and H. M. Li, *Electrochim. Acta*, 2019, **293**, 426–431.
69 L. Li, S. Kim, W. Wang, M. Vijayakumar, Z. Nie, B. Chen, J. Zhang, G. Xia, J. Hu, G. Graff, J. Liu and Z. Yang, *Adv. Energy Mater.*, 2011, **1**, 394–400.
70 M. J. Taylor and J. M. Coddington, *Polyhedron*, 1992, **11**, 1531–1544.
71 Y.-N. Li, J.-Q. Wang, L.-N. He, Z.-Z. Yang, A.-H. Liu, B. Yu and C.-R. Luan, *Green Chem.*, 2012, 2752–2758.
72 A. S. Amarasekara, *Chem. Rev.*, 2016, **116**, 6133–6183.
73 E. I. Izgorodina and D. R. MacFarlane, *J. Phys. Chem. B*, 2011, **115**, 14659–14667.
74 Y. J. Kim and R. S. Varma, *J. Org. Chem.*, 2005, **70**, 7882–7891.

75 S. Minomura and H. G. Drickamer, *J. Chem. Phys.*, 1961, **35**, 903–907.
76 Y. Wang, H. Li and S. Han, *J. Chem. Phys*, 2005, **123**, 174501.
77 S. Tsuzuki, R. Katoh and M. Mikami, *Mol. Phys.*, 2008, **106**, 1621–1629.
78 S. Tsuzuki, H. Tokuda and M. Mikami, *Phys. Chem. Chem. Phys.*, 2007, 4780–4784.
79 H. Weingärtner, *Angew. Chemie - Int. Ed.*, 2008, **47**, 654–670.
80 Z. J. Chen, T. Xue and J.-M. Lee, *RSC Adv.*, 2012, 10564–10574.
81 S. Schaltin, P. Nockemann, B. Thijs, K. Binnemans and J. Fransaer, *Electrochem. Solid-State Lett.*, 2007, **10**, D104.
82 Y. Ye and Y. A. Elabd, *Polymer*, 2011, 1309–1317.
83 J. K. Puri and R. Chhoker, *J. Chem.*, 2013, **2013**, 1–9.
84 A. A. Mohamed, *Coord. Chem. Rev.*, 2010, **254**, 1918–1947.
85 D. Forster and D. M. L. Goodgame, *Inorg. Chem.*, 1965, **4**, 823–829.
86 M. D. Fryzuk, D. B. Leznoff, R. C. Thompson and S. J. Rettig, *J. Am. Chem. Soc.*, 1998, **120**, 10126–10135.
87 B. R. Hollebone and R. S. Nyholm, *J. Chem. Soc. A Inorganic, Phys. Theor.*, 1971, **120**, 332.
88 S. Wellens, B. Thijs and K. Binnemans, *Green Chem.*, 2012, 1657.
89 T. Ueda, T. Tominaga, T. Mochida, K. Takahashi and S. Kimura, *Chem Eur. J.*, 2018, 9490–9493.
90 Y. Funasako, S. Mori and T. Mochida, *Chem. Commun.*, 2016, **52**, 6277–6279.
91 J. Estager, J. D. Holbrey and M. Swadźba-Kwaśny, *Chem. Soc. Rev.*, 2014, **43**, 847-886 .
92 J. Estager, P. Nockemann, K. R. Seddon, M. Swad Zba-Kwa and S. Tyrrell, *Inorg. Chem*, 2011, **50**, 16.
93 K. Dong, X. Liu, H. Dong, X. Zhang and S. Zhang, *Chem. Rev.*, 2017, 6636–6695.
94 M. A. Gebbie, A. M. Smith, H. A. Dobbs, A. A. Lee, G. G. Warr, X. Banquy, M. Valtiner, M. W. Rutland, J. N. Israelachvili, S. Perkin and R. Atkin, *Chem. Commun*, 2017, **53**, 1214.
95 T. Ogawa, K. Takahashi, S. S. Nagarkar, K. Ohara, Y.-L. Hong, Y. Nishiyama and S. Horike, 2020, **11**, 5175-5181.
96 N. Ogiwara, M. Inukai, T. Itakura, S. Horike and S. Kitagawa, *Chem. Mater.*, 2016, **28**, 3968–3975.
97 K. Ueno, H. Tokuda, M. Watanabe, Y. Yoshida, G. Saito, N. Wood, G. Stephens, D. R. MacFarlane, J. M. Pringle, P. C. Howlett, M. Forsyth, R. Hayes, G. G. Warr, R. Atkin, P. Chem, H. Liu, Y. Liu, J. Li, P. Chem Chem, O. Höfft, N. Borisenko, L. Henrique Gasparotto, A. Prowald, R. Al-Salman, T. Carstens, A. Bund, S. Zein El Abedin, M. Brettholle, O. Höfft, L. Klarhöfer, S. Mathes, W. Maus-Friedrichs, S. Zein El Abedin, S. Krischok, J. Janek, T. Kameyama, Y. Ohno, T. Kurimoto, K. Okazaki, T. Uematsu, S. Kuwabata, C. Krekeler, F. Dommert, J. Schmidt, Y. Y. Zhao, C. Holm, R. Berger, L. Delle, J. Min Lee, J. Palgunadi, J. Hyung Kim, S. Jung, Y. Choi, M. Cheong, H. Sik Kim, A. P. Abbott, F. Qiu, H. M. A Abood, M. Rostom Ali, K. S. Ryder, B. C. M Martindale, S. E. Ward Jones, S. Glyn Jones, H. Man Yau, E. Davies, J. M. Hook, T. G. A Youngs, J. B. Harper, A. K. Croft, Y. Cui, I. Biondi, M. Chaubey, X. Yang, Z. Fei, R. Scopelliti, C. G. Hartinger, Y. Li, C. Chiappe, P. J. Dyson, K. Lunstroot, K. Driesen, P. Nockemann, L. Viau, P. Hubert Mutin, A. Vioux, K. Binnemans, S. Hayaki, K. Kido, H. Sato, S. Sakaki, V. Strehmel, H. Rexhausen, P. Strauch, B. M. Sato, C. G. de Oliveira, C. T. Martins and O. A. El, *Phys. Chem. Chem. Phys.*, 2010, **12**, 1648.

98 H. Li, M. Ibrahim, I. Agberemi and M. N. Kobrak, *Crit. Rev. J. Phys. Chem. Ref. Data*, 2008, **129**, 33101.
99 J. L. Anderson, J. Ding, T. Welton and D. W. Armstrong, *J. Am. Chem. Soc*, 2002, 14247–14254.
100 L. Xiao, J. S. Wilkes and K. E. Johnson, *ECS Proc. Vol.*, 2002, **2002**–**19**, 964–972.
101 S. Mecozzi and J. Rebek, Jr., *Chem—Eur. J.*, 1998, **4**, 1016–1022.
102 E. C. Sutton, C. E. Mcdevitt, J. Y. Prochnau, M. V Yglesias, A. M. Mroz, M. C. Yang, R. M. Cunningham, C. H. Hendon and V. J. Derose, *J. Am. Chem. Soc*, 2019, **141**, 28.
103 C. E. Mcdevitt, M. V Yglesias, A. M. Mroz, E. C. Sutton, M. C. Yang, C. H. Hendon and V. J. Derose, *JBIC J. Biol. Inorg. Chem.*, 2019, **24**, 899–908.

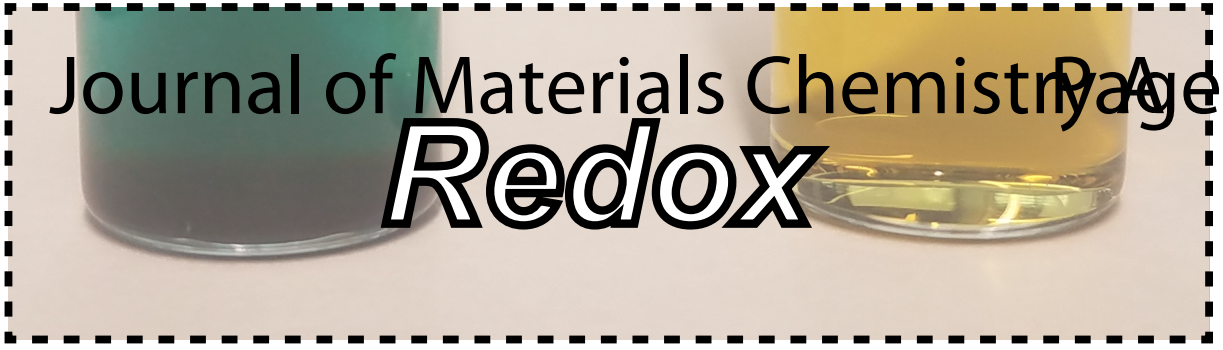

$$4[P_{6,6,6,14}][VCl_4] + O_2 + 4H_2O \longrightarrow 4[P_{6,6,6,14}][H][O{=}VCl_4] + 2H_2O$$

$$[P_{6,6,6,14}]_2[CoCl_4] + 4HBr_{(aq)} \longrightarrow [P_{6,6,6,14}]_2[CoBr_4] + 4H{\bullet}Cl$$